Proceedings of the XXVI Iberian Latin-American Congress on Computational Methods in Engineering – CILAMCE 2005
Brazilian Assoc. for Comp. Mechanics (ABMEC) & Latin American Assoc. of Comp. Methods in Engineering (AMC),
Guarapari, Espírito Santo, Brazil, 19th – 21st October 2005

Paper CIL 16-0008

A DISCONTINUOUS FINITE ELEMENT METHOD AT ELEMENT LEVEL APPLIED TO HELMHOLTZ EQUATION WITH MINIMAL POLLUTION

Abimael Fernado Dourado Loula
aloc@lncc.br
LNCC – Laboratório Nacional de Computação Científica
Getulio Vargas 333 – Quitandinha – 25651-070 – Petrópolis, RJ, Brasil

Gustavo Benitez Alvarez
benitez.gustavo@gmail.com
DCET/UESC – Universidade Estadual de Santa Cruz
Rodovia Ilhéus-Itabuna, Km 16 – 45.650-000 – Ilhéus, BA, Brasil

Eduardo Gomes Dutra do Carmo
Fernando Alves Rochinha
egdcarmo@hotmail.com
rochinha@adc.coppe.ufrj.br
COPPE/UFRJ – Universidade Federal do Rio de Janeiro
Ilha do Fundão – 21945-970 – P.B. 68509 – Rio de Janeiro, RJ, Brasil

Abstract. *A discontinuous finite element formulation is presented for Helmholtz equation. Continuity is relaxed locally in the interior of the element instead of across the element edges. Discontinuities are introduced locally, inside each element, through C^1 shape functions associated with interior nodes. The interior shape functions can be viewed as discontinuous bubbles and the corresponding degrees of freedom can be eliminated at element level by static condensation yielding a global matrix topologically equivalent to those of classical C^0 finite element approximations. A crucial point of the discontinuous formulation relies on the choice of the stabilization parameters related to the weak enforcement of continuity inside each element. Explicit values of these stabilization parameters minimizing the pollution effect are presented for uniform meshes. The accuracy and stability of the proposed formulation for bilinear shape functions are demonstrated in several numerical examples.*

Keywords: *Discontinuous bubbles, Helhmoltz equation, Stabilization, Discontinuous finite element method*

1. INTRODUCTION

Time-harmonic acoustic, elastic and electromagnetic waves are governed by the Helmholtz equation. Numerical approximation of this equation is particularly challenging as reported in a vast literature. The oscillatory behavior of the exact solution and the quality of the numerical approximation depend on the wave number k. To approximate Helmholtz equation with acceptable accuracy the resolution of the mesh should be adjusted to the wave number according to the rule of thumb (Harari et al, 1991), which prescribes a minimum number of elements per wavelength. It is well known that, despite of the adoption of this rule, the performance of the Galerkin finite element method deteriorates as k increases. This misbehavior, known as pollution of the finite element solution (Ihlenburg et al, 1995;

Babuška et al, 1995), can only be avoided after a drastic refinement of the mesh, which normally entails significant barriers for the numerical analysis of Helmholtz equation at mid and high frequencies.

A great effort has been devoted to alleviate the pollution effect (see references). In particular, the GLS method (Galerkin Least-Squares) is able to completely eliminate the phase lag in one dimension problems (Harari et al, 1992). Nevertheless, in two-dimensions this method is not pollution-free for any direction of a plane wave (Thompson et al, 1995). In fact, in two space dimensions, there is no finite element method with piecewise linear shape functions free of pollution effect. Stencils with minimal pollution error are constructed in (Babuška et al, 1995) through the Quasi Stabilized Finite Element Method (QSFEM). The QSFEM is really a finite difference rather than a finite element method. The modifications of the discrete operator are made on the algebraic level and no variational formulation is associated with the QSFEM presented in (Babuška et al, 1995).

Recently, we introduced a discontinuous finite element formulation for Helmholtz equation depending on two stabilization parameters (Alvarez et al, submitted). Several numerical experiments show the good performance and potential of this formulation to reduce the pollution effect. Completely discontinuous formulation, as presented in (Alvarez et al, submitted) , may lead to high computational cost since the degrees of freedom associated with the discontinuity can not be eliminated. Moreover, the two parameters of this formulation (β and λ) are determined through numerical experiments.

The new method contained in the present work is also based on a discontinuous finite element formulation (Dutra do Carmo et al, 2002; Alvarez et al, submitted), but now the continuity is relaxed only on the interiors of elements instead of across the element edges as it was admitted in our previous formulation (Loula et al, submitted). Continuity on the interelement boundaries is enforced considering C^0 Lagrangian interpolation globally as usual. Discontinuities are introduced locally, inside each element, through C^1 shape functions associated with interior nodes with zero value on the element boundary. Thus, the interior shape functions can be viewed as discontinuous bubbles and the corresponding degrees of freedom can be eliminated at element level by static condensation yielding a global matrix topologically equivalent to those of classical C^0 finite element approximations. Again, a crucial point of the discontinuous formulation relies on the choice of the stabilization parameters (β and λ) related to the weak enforcement of continuity inside each element. For uniform meshes we present a methodology to determine explicitly the stabilization parameters minimizing the pollution effect. In particular, the QSFEM stencil emanates consistently from the proposed variational formulation by an appropriate choice of these parameters.

2. THE HELMHOLTZ EQUATION

2.1 The boundary value problem

Let $\Omega \subset R^n$ be an open bounded domain with a Lipschitz continuous smooth piecewise boundary Γ. Let Γ_g, Γ_q, Γ_r be three disjoint subsets of Γ where boundary conditions are specified, such that $\Gamma_g \cup \Gamma_q \cup \Gamma_r = \Gamma$. We shall consider the interior Helmholtz problem:

$$-\nabla \cdot (\nabla u) - k^2 u = f \quad \text{in } \Omega, \tag{1}$$

$$u = g \quad \text{on } \Gamma_g, \tag{2}$$

$$\nabla u \cdot \hat{n} = q \quad \text{on } \Gamma_q, \tag{3}$$

$$\nabla u \cdot \hat{n} + \alpha u = r \quad \text{on } \Gamma_r, \tag{4}$$

where u denotes a scalar field that describes time-harmonic acoustic, elastic or electromagnetic steady state waves. The coefficient $k \in R$ is the wave number, $f \in L^2(\Omega)$ is the source term, $g \in H^{\frac{1}{2}}(\Gamma_g) \cap C^0(\Gamma_g)$, $q \in L^2(\Gamma_q)$ and $r \in L^2(\Gamma_r)$ are the prescribed boundary conditions. The coefficient $\alpha \in L^\infty(\Gamma_r)$ is positive on Γ_r and $\hat{n}$ denotes the outward normal unit vector defined almost everywhere on Γ.

2.2 Variational boundary-value problem

The variational formulation of the boundary value problem defined as Eq. (1) to Eq. (4), involves finding $u \in S$ that satisfies the variational equation:

$$\int_\Omega [(\nabla u)\cdot \nabla v - k^2 uv]\, d\Omega - \int_{\Gamma_q} qv\, d\Gamma + \int_{\Gamma_r} (\alpha u - r) v\, d\Gamma = \int_\Omega f\, v\, d\Omega \quad \forall\, v \in V, \tag{5}$$

where $S = \{u \in H^1(\Omega): u = g \text{ on } \Gamma_g\}$ denotes the set of admissible solution and $V = \{v \in H^1(\Omega): v = 0 \text{ on } \Gamma_g\}$ the space of the admissible test functions.

2.3 The continuous Galerkin and GLS finite element formulations

Consider $M^h = \{\Omega_1, \ldots, \Omega_{NE}\}$ a finite element partition of Ω, such that: $\overline{\Omega} = \Omega \cup \Gamma = \bigcup_{E=1}^{NE} \overline{\Omega}_E = \bigcup_{E=1}^{NE} (\Omega_E \cup \Gamma_E)$, $\Omega_E \cap \Omega_{E'} = \emptyset$ if $E \neq E'$ and Γ_E denotes the boundary of Ω_E. The continuous finite element set and space of S and V are defined as: $S^l_{h,a} = \{u^{h,a} \in H^1(\Omega): u^{h,a}_E \in P^l(\Omega_E),\ u^{h,a} = g^h \text{ on } \Gamma_g\}$ and $V^l_{h,a} = \{v^{h,a} \in H^1(\Omega): v^{h,a}_E \in P^l(\Omega_E),\ v^{h,a} = 0 \text{ on } \Gamma_g\}$, where $P^l(\Omega_E)$ is the space of polynomials of degree less than or equal to l, g^h denotes the interpolation of g and $u^{h,a}_E$ denotes the restriction of $u^{h,a}$ to Ω_E.

Problem Eq. (5) have been approximated by the following finite element methods: find $u^h \in S^l_{h,a}$ that satisfies $\forall v^h \in V^l_{h,a}$,

Galerkin method

$$A_G(u^h, v^h) = F_G(v^h), \tag{6}$$

$$A_G = \sum_{E=1}^{NE} \int_{\Omega_E} [\nabla u^h_E \cdot \nabla v^h_E - k^2 u^h_E\, v^h_E]\, d\Omega + \int_{\Gamma_r} \alpha u^h v^h\, d\Gamma, \tag{7}$$

$$F_G = \sum_{E=1}^{NE} \int_{\Omega_E} f\, v^h_E\, d\Omega + \int_{\Gamma_q} q v^h\, d\Gamma + \int_{\Gamma_r} r v^h\, d\Gamma,$$

Galerkin Least-Squares method (GLS)

$$A_G(u^h, v^h) + A_{LS}(u^h, v^h) = F_G(v^h) + F_{LS}(v^h), \tag{8}$$

$$A_{LS} = \sum_{E=1}^{NE} \int_{\Omega_E} [-\nabla\cdot(\nabla u^h_E) - k^2 u^h_E]\, p^h_E\, d\Omega, \quad F_{LS} = \sum_{E=1}^{NE} \int_{\Omega_E} f_E\, p^h_E\, d\Omega, \tag{9}$$

$$p^h_E = \tau_E \left[-\nabla\cdot(\nabla v^h_E) - k^2 v^h_E\right] \quad \forall \Omega_E \in M^h, \tag{10}$$

$$\tau_E = \frac{1}{k^2}\left[1 - 6\frac{4-\cos\zeta_1 - \cos\zeta_2 - 2\cos\zeta_1\cos\zeta_2}{(2+\cos\zeta_1)(2+\cos\zeta_2)k^2h^2}\right], \quad \zeta_1 = kh\cos\theta, \quad \zeta_2 = khsin\theta. \quad (11)$$

In one-dimension space, the GLS method eliminate the phase error (Harari et al, 1992). In two-dimensions, this method is not pollution-free for any θ directions of a plane wave (Thompson et al, 1995).

3. THE DISCONTINUOUS FINITE ELEMENT METHOD AT ELEMENT LEVEL

Consider for each element $\Omega_E \in M^h$ a subgrid $\overline{\Omega}_E = \bigcup_{e=1}^{ne} \Omega_E^e \cup \Gamma_E^e$, where Γ_E^e denotes the boundary of Ω_E^e. Introducing in each macroelement Ω_E the discontinuous finite element subspaces, $V_{h,b}^l = \{v^{h,b} \in L^2(\Omega_E) : v_{E,e}^{h,b} \in P^l(\Omega_E^e) \text{ and } v_{E,e}^{h,b} = 0 \text{ on } \Gamma_E^e \cap \Gamma_E = \emptyset\}$, the discontinuous finite element method at element level consists in finding $u^h = (u^{h,a} + u^{h,b}) \in S_{h,a}^l + S_{h,b}^l$ satisfying two equations:

$$A_{DG}(u^{h,a} + u^{h,b}, v^{h,a}) = F_G(v^{h,a}) \qquad \forall v^{h,a} \in V_{h,a}^l, \quad (12)$$

$$A_{DG}(u^{h,a} + u^{h,b}, v^{h,b}) = F_G(v^{h,b}) \qquad \forall v^{h,b} \in V_{h,b}^l, \quad (13)$$

where $A_{DG}(u^h, v^h)$ and $F_G(v^h)$ are given by

$$A_{DG}(u^h, v^h) = \sum_{E=1}^{NE} A_E(u_E^h, v_E^h) + \int_{\Gamma_r} \alpha u^h v^h \, d\Gamma, \quad (14)$$

$$F_G(v^h) = \sum_{E=1}^{NE} F_E(v_E^h) + \int_{\Gamma_q} q v^h \, d\Gamma + \int_{\Gamma_r} r v^h \, d\Gamma, \quad (15)$$

$$A_E(u_E^h, v_E^h) = \sum_{e=1}^{ne} \int_{\Omega_E^e} [\nabla u_E^h \cdot \nabla v_E^h - k^2 u_E^h v_E^h] \, d\Omega +$$

$$+ \sum_{e=1}^{ne} \sum_{\substack{e'>e \\ \Gamma_E^{ee'} \neq \emptyset}}^{ne} \int_{\Gamma_E^{ee'}} \left[\frac{\beta_E^{ee'}}{h_{ee'}} (u_{E,e}^h - u_{E,e'}^h)(v_{E,e}^h - v_{E,e'}^h) + \frac{\lambda_E^{ee'}}{2} (u_{E,e}^h - u_{E,e'}^h)(\nabla v_{E,e}^h \cdot \hat{n}_E^e - \nabla_{E,e'}^h \cdot \hat{n}_E^{e'}) \right.$$

$$\left. - \frac{1}{2} (\nabla u_{E,e}^h \cdot \hat{n}_E^e - \nabla u_{E,e'}^h \cdot \hat{n}_E^{e'})(v_{E,e}^h - v_{E,e'}^h) \right] d\Gamma, \quad (16)$$

$$F_E(v_E^h) = \sum_{e=1}^{ne} \int_{\Omega_E^e} f_{E,e} \, v_{E,e}^h \, d\Omega, \quad (17)$$

$u_{E,e}^h$ denotes the restriction u^h to element Ω_E^e, $\Gamma_E^{e,e'} = \Gamma_E^e \cap \Gamma_E^{e'}$, $\hat{n}_E^e$ is the outward normal unit vector to Γ_E^e, $h_{ee'} = \min\{h_{E,e}, h_{E,e'}\}$, where $h_{E,e}$ and $h_{E,e'}$ are the subgrid mesh parameters. This formulation is consistent in the sense that the exact solution u of problem Eq.(1-4) is also solution of Eq.(12-13).

The space $V_{h,a}^l + V_{h,b}^l$ can be understood as classical finite element space $V_{h,a}^l$ enriched with discontinuous bubble functions within each macroelement. Bubbles functions are typically higher-order polynomials defined on the interiors of each element, which vanish on element boundaries. Note that, for this case, these bubble functions do not need to be higher-order polynomials ($l \geq 1$). The degrees of freedom associated with bubbles can be eliminated by the know 'static condensation'. Moreover, the continuity in this formulation is relaxed on the interiors of elements (subgrid) depending on $\beta_E^{ee'}$ and $\lambda_E^{ee'}$ parameters. Initially, these parameters were introduced in (Dutra do carmo et al, 2002; Alvarez et al, submitted) and its choice is crucial for the quality of the numerical solution. Here, $\beta_E^{ee'}$ and $\lambda_E^{ee'}$ parameters will be determined in order to reduce the pollution effects of the numerical solution.

3.1 Condensation of the Subgrid Degrees of Freedom

The finite element system Eq. (12) and Eq. (13) in matrix form is given by

$$AU_a + B(\widetilde{\lambda})U_b = F_a, \qquad CU_a + D(\widetilde{\lambda},\widetilde{\beta})U_b = F_b \tag{18}$$

where A, $B(\widetilde{\lambda})$, C and $D(\widetilde{\lambda},\widetilde{\beta})$ are global matrices, F_a and F_b are the global vectors of source term, U_a is the vector of global unknowns of the coarse mesh, U_b is the vector of subgrid unknowns, $\widetilde{\lambda},\widetilde{\beta} = \{\lambda_E^{ee'}, \beta_E^{ee'}\ e,e'=1,\ldots,ne;\ E=1,\ldots NE\}$ are the two set of parameters related to the weak enforcement of continuity on the interface $\Gamma_E^{ee'}$ of the elements Ω_E^e and $\Omega_E^{e'}$ in each macroelement Ω_E. For given $\widetilde{\lambda}$ and $\widetilde{\beta}$ the matrix $D(\widetilde{\lambda},\widetilde{\beta})$ can be easily inverted for being block diagonal a direct consequence of choosing $v^{h,b}$ bubble-like functions. Eliminating the vector U_b in system Eq. (18) we obtain the condensed global system

$$A^*U_a = F^*, \quad A^* = A - B(\widetilde{\lambda})D(\widetilde{\lambda},\widetilde{\beta})^{-1}C, \quad F^* = F_a - B(\widetilde{\lambda})D(\widetilde{\lambda},\widetilde{\beta})^{-1}F_b, \tag{19}$$

which is topologically equivalent to that corresponding to the classical C^0 Galerkin approximation in the macro mesh. In fact the subgrid degrees of freedom are eliminated at macroelement level, and the condensed global system is obtained by adding the corresponding macroelement contributions

$$A_E^* = A_E - B_E(\widetilde{\lambda})D_E(\widetilde{\lambda},\widetilde{\beta})^{-1}C_E, \quad F_E^* = F_{a,E} - B_E(\widetilde{\lambda})D_E(\widetilde{\lambda},\widetilde{\beta})^{-1}F_{b,E}. \tag{20}$$

In the next section we determined explicitly the sets of parameters $\widetilde{\lambda}$ and $\widetilde{\beta}$ by minimizing the phase lag for a uniform mesh. At that point it is important to mention that enriching the approximation space with the discontinuous bubbles has as a primary goal to provide stability to the discrete formulation. The great gain in accuracy of the proposed formulation compared to the standard C^0 Galerkin and Galerkin Least Squares methods, as illustrated in section 4, is only due to the additional stability of the discontinuous formulation which is capable to minimize pollution effects. In this aspect our approach differs from the residual free bubble formulation for Helmholtz equation presented in (Franca et al, 1997).

3.2 Optimal Choice of the Stabilization Parameters

For simplicity we now consider only bilinear polynomial interpolations and uniform mesh with square macroelements of length h composed by a subgrid with four square elements of length $\frac{h}{2}$. Thus we have 8 degrees of freedom per macroelements: 4

corresponding to $u^{h,a}$ and the other 4 corresponding to $u^{h,b}$ that will be condensed at the macroelement level. We observe that, for this particular mesh, $\lambda_E^{e,e'} = \lambda$, $\beta_E^{e,e'} = \beta$ and the local matrices are given explicitly by

$$A_E = \sum_{i=0}^{2} a_i E_i,\ B_E = \sum_{i=0}^{2} b_i(\lambda) E_i,\quad C_E = \sum_{i=0}^{2} c_i E_i,\ D_E = \sum_{i=0}^{2} d_i(\lambda,\beta) E_i, \tag{21}$$

where E_i (*i=0,1,2*) are the following *4×4* matrices

$$E_0 = I = \begin{bmatrix} 1 & 0 & 0 & 0 \\ 0 & 1 & 0 & 0 \\ 0 & 0 & 1 & 0 \\ 0 & 0 & 0 & 1 \end{bmatrix},\ E_1 = \begin{bmatrix} 0 & 1 & 0 & 1 \\ 1 & 0 & 1 & 0 \\ 0 & 1 & 0 & 1 \\ 1 & 0 & 1 & 0 \end{bmatrix},\ E_2 = \begin{bmatrix} 0 & 0 & 1 & 0 \\ 0 & 0 & 0 & 1 \\ 1 & 0 & 0 & 0 \\ 0 & 1 & 0 & 0 \end{bmatrix} \tag{22}$$

and

$$a_0 = \frac{2}{3} - \alpha_G,\quad a_1 = -\frac{1}{6} - \frac{\alpha_G}{2},\quad a_2 = \frac{1}{3} - \frac{\alpha_G}{4}, \tag{23}$$

$$b_0 = -\frac{\alpha_G}{4} - \frac{\lambda+1}{3},\quad b_1 = -\frac{\alpha_G}{8} + \frac{\lambda+1}{12},\quad b_2 = -\frac{\alpha_G}{16} + \frac{\lambda+1}{6}, \tag{24}$$

$$c_0 = -\frac{\alpha_G}{4},\quad c_1 = -\frac{\alpha_G}{8},\quad c_2 = -\frac{\alpha_G}{16},\quad d_0 = \gamma + 2\mu,\quad d_1 = -\mu,\quad d_2 = 0, \tag{25}$$

with $\alpha_G = \frac{(kh)^2}{9}$, $\gamma = \frac{2}{3} - \frac{\alpha_G}{4}$, $\mu = \frac{2\beta + \lambda - 1}{6}$.

Solving the eigenproblem

$$XV = wV,\ \text{with}\ X = \sum_{i=0}^{2} x_i E_i, \tag{26}$$

we obtain the eigenvalues $w_1^x = x_0 + 2x_1 + x_2$, $w_2^x = w_3^x = x_0 - x_2$, $w_1^x = x_0 - 2x_1 + x_2$, and the matrix of the eigenvectors

$$M = \frac{1}{2}\begin{bmatrix} 1 & 1 & 1 & 1 \\ 1 & 1 & -1 & -1 \\ 1 & -1 & -1 & 1 \\ 1 & -1 & 1 & -1 \end{bmatrix}\ \text{with}\ MM^T = M^T M = I.$$

Using the matrix equation $A_E^* = \sum_{i=0}^{2} a_i^* E_i = A_E - B_E(\lambda) D_E(\lambda,\beta)^{-1} C_E$ in the diagonal form

$$M^T A_E^* M = M^T A_E M - M^T B_E(\lambda) D_E(\lambda,\beta)^{-1} C_E M,$$

or equivalently, $w^{a_i^*} = w^{a_i} - w^{b_i} w^{c_i} / w^{d_i}$, $i = 1,2,3,4$, we obtain the following algebraic system of three independent equations

$$a_0^* + 2a_1^* + a_2^* = -\frac{9\alpha_G}{4} - \left[\frac{9\alpha_G}{16}\right]^2 \frac{1}{\gamma}, \tag{27}$$

$$a_0^* - a_2^* = 1 - \frac{3\alpha_G}{4} - \frac{3\alpha_G}{16}\left[\frac{3\alpha_G}{16} + \frac{\lambda+1}{2}\right]\frac{1}{\gamma+2\mu}, \tag{28}$$

$$a_0^* - 2a_1^* + a_2^* = \frac{2}{3} - \frac{\alpha_G}{4} - \frac{\alpha_G}{16}\left[\frac{\alpha_G}{16} + \frac{\lambda+1}{3}\right]\frac{1}{\gamma+4\mu}, \tag{29}$$

relating the coefficients of the condensed matrix A_E^* and the stabilization parameters.

Now, using discrete Fourier transform in the homogeneous form of the global system corresponding to the present uniform mesh, the stencil of an interior node leads to

$$a_2^*\tilde{r} + a_0^* + a_1^*\tilde{w} = 0 \tag{30}$$

with $\tilde{r} = \cos(\tilde{k}h\cos\theta)\cos(\tilde{k}hsin\theta)$, $\tilde{w} = \cos(\tilde{k}h\cos\theta) + \cos(\tilde{k}hsin\theta)$ where θ is the direction of a plane wave, and k is the discrete wavelength. We should observe that the coefficients $a_i^*, i = 0,1,2,$ depend on k and h, and on the free parameters λ and β. Thus we have the freedom to choose λ and β to minimize the phase lag. We then choose two directions θ_1 and θ_2 such that the dispersion relation Eq. (30) is verified for $\tilde{k} = k$, yielding

$$a_2^* r_1 + a_0^* + a_1^* w_1 = 0, \tag{31}$$

$$a_2^* r_2 + a_0^* + a_1^* w_2 = 0, \tag{32}$$

with

$$r_1 = \cos(kh\cos\theta_1)\cos(khsin\theta_1),\ r_2 = \cos(kh\cos\theta_2)\cos(khsin\theta_2), \tag{33}$$

$$w_1 = \cos(kh\cos\theta_1) + \cos(khsin\theta_1),\ w_2 = \cos(kh\cos\theta_2) + \cos(khsin\theta_2), \tag{34}$$

Solving the algebraic system Eq. (27-29, 31-32) of five independent equations we obtain the following expressions for the stabilization parameters:

$$\lambda = -1 + \frac{(p_3 g_1 - p_1 g_3)}{(p_2 g_1 - p_1 g_2)}, \tag{35}$$

$$\beta = 1 + 3\frac{(p_2 g_3 - p_3 g_2)}{(p_2 g_1 - p_1 g_2)} - \frac{1}{2}\frac{(p_3 g_1 - p_1 g_3)}{(p_2 g_1 - p_1 g_2)}, \tag{36}$$

and for the coefficients of the condensed matrix A_E^*:

$$a_0^* = \frac{(r_2 w_1 - r_1 w_2)(576\alpha_G\gamma + 81\alpha_G{}^2)}{256\gamma\left[r_2 w_1 - r_1 w_2 + 2(r_1 - r_2) + w_2 - w_1\right]}, \tag{37}$$

$$a_1^* = a_0^* \frac{(r_1 - r_2)}{(r_2 w_1 - r_1 w_2)}, \tag{38}$$

$$a_2^* = a_0^* \frac{(w_1 - w_2)}{(r_2 w_1 - r_1 w_2)}, \tag{39}$$

with

$$g_1 = -4(a_1^* + a_2^*) - 2\left[1 + 24p_0 + \frac{81}{\gamma} p_0{}^2\right],\ p_0 = \frac{\alpha_G}{16}, \tag{40}$$

$$g_2 = \frac{3p_0}{2},\ \ g_3 = \gamma\left[2(a_1^* + a_2^*) + 1 + 24p_0 + \frac{81}{\gamma} p_0{}^2\right] - 9p_0{}^2, \tag{41}$$

$$p_1 = -16a_1^* - 4\left[\frac{2}{3} + 32p_0 + \frac{81}{\gamma} p_0{}^2\right], \tag{42}$$

$$p_2 = \frac{p_0}{3},\ \ p_3 = \gamma\left[4a_1^* + \frac{2}{3} + 32p_0 + \frac{81}{\gamma} p_0{}^2\right] - p_0{}^2. \tag{43}$$

Due to the symmetry of the uniform mesh θ_1 and θ_2 should be chosen such that $\theta_1, \theta_2 \in (0, \frac{\pi}{4})$ with $\theta_1 \neq \theta_2$ and $\theta_1 - \theta_2 \neq \frac{\pi}{4}$ to avoid an indefinite system for λ and β. We should note that the approximate solution is pollution-free only if the exact solution is a plane wave in direction θ_1 or θ_2. For any other direction different from θ_1 or θ_2, when the wave number *k* is increased pollution effects appear, as will be shown in the numerical tests.

From equations Eq. (31) and Eq. (32) we observe that choosing $\theta_1 = \frac{\pi}{16}$ and $\theta_2 = \frac{3\pi}{16}$, the condensed element matrix of the present discontinuous finite element formulation generates an interior stencil identical to that of the Quasi Stabilized Finite Element Method (QSFEM) with minimal pollution error compared to any nine point stencil (or any C^0 four node element) as presented in (Babuška et al, 1995). Figure 1 plots λ and β parameters as a function of *kh* obtained with $\theta_1 = \frac{\pi}{16}$ and $\theta_2 = \frac{3\pi}{16}$.

The stabilization parameters (λ and β) and the coefficients of the condensed matrix (A_E^*) can be expanded as a Taylor series. The coefficients of Taylor expansion about a point *kh=0.5* are present in Table 1.

The dispersion relation Eq. (30) leads to a phase lag $\left|k - \tilde{k}\right|$ depending on *kh* and θ. In Fig. 2 we compare the exact and approximate dispersion relations corresponding to three finite element approximations: the classical Galerkin method (CG), the Galerkin Least-Squares (GLS) with $\tau(\theta = \frac{\pi}{8})$, as presented in (Thompson et al, 1995), and the present discontinuous bubble formulation (DGB), for *kh=1*. We observe no visual difference between the dispersion relation of DGB and the exact one (case b).

4. NUMERICAL RESULTS

We present in this section three 2-D examples to illustrate the performance of the proposed discontinuous formulation applied to Helmholtz problem. In all examples bilinear shape functions and 2x2 Gaussian integration are adopted combined with the optimal choice of the stabilization parameters given by equations Eq. (35) and Eq. (36) with $\theta_1 = \frac{\pi}{16}$ and $\theta_2 = \frac{3\pi}{16}$.

For the convergence study, we introduce relative errors of the continuous $u^{h,a}$ of the finite element approximation in L^2-norm and H^1-seminorm:

$$\|RE\|_{L^2(\Omega)} = \frac{\left\|u^{ex} - u^{h,a}\right\|_{L^2(\Omega)}}{\left\|u^{ex}\right\|_{L^2(\Omega)}}, \quad |RE|_{H^1(\Omega)} = \frac{\left|u^{ex} - u^{h,a}\right|_{H^1(\Omega)}}{\left|u^{ex}\right|_{H^1(\Omega)}}.$$

The additional accuracy provided by the contribution $u^{h,b}$ of the discontinuous bubbles to the finite element solution $u^{h,b}$ is only marginal and will not be considered in this study.

Table 1. Coefficients of Taylor serires for λ, β and A_E^*

<table>
<tr><td rowspan="2">n</td><td colspan="4">$f(x) = \sum_{n=0}^{9} \frac{f^{(n)}(x_o)}{n!}(x - x_o)^n + O(x^{10})$, where $x = kh$ and $x_o = 0.5$</td></tr>
<tr><td colspan="2">λ</td><td colspan="2">β</td></tr>
<tr><td>0</td><td colspan="2">0.8713704950767354</td><td colspan="2">-0.4317471787080831</td></tr>
<tr><td>1</td><td colspan="2">-0.18213416553844297</td><td colspan="2">0.10672708182473101</td></tr>
<tr><td>2</td><td colspan="2">-0.18597491289271417</td><td colspan="2">0.10826792756269055</td></tr>
<tr><td>3</td><td colspan="2">-0.007842665723494235</td><td colspan="2">0.0031191985941498857</td></tr>
<tr><td>4</td><td colspan="2">-0.004350288276611991</td><td colspan="2">0.0016609079390352832</td></tr>
<tr><td>5</td><td colspan="2">-0.0005375125198270325</td><td colspan="2">0.00011689601784681258</td></tr>
<tr><td>6</td><td colspan="2">-0.0002685676729470287 7</td><td colspan="2">0.00005459962332565737 6</td></tr>
<tr><td>7</td><td colspan="2">-0.000034794064276866266</td><td colspan="2">-0.000012440594417739703</td></tr>
<tr><td>8</td><td colspan="2">-0.00008085841000138316</td><td colspan="2">0.00002601229044785213 8</td></tr>
<tr><td>9</td><td colspan="2">-1.341153620160184810^{-6}</td><td colspan="2">-5.275705461826873910^{-6}</td></tr>
<tr><td></td><td>a_0^*</td><td colspan="2">a_1^*</td><td>a_2^*</td></tr>
<tr><td>0</td><td>0.79164791402110091</td><td colspan="2">-0.34094683985104524</td><td>-0.17262430010848387</td></tr>
<tr><td>1</td><td>-0.16690365594732715</td><td colspan="2">-0.030876505682349231</td><td>-0.024319440721215946</td></tr>
<tr><td>2</td><td>-0.16753986179438707</td><td colspan="2">-0.032591537819737892</td><td>-0.026299533042878798</td></tr>
<tr><td>3</td><td>-0.0012576018400359545</td><td colspan="2">-0.0034987524703067319</td><td>-0.0040922017882303319</td></tr>
<tr><td>4</td><td>-0.00055719318502756021</td><td colspan="2">-0.001956668301353881</td><td>-0.002350303014317045 6</td></tr>
<tr><td>5</td><td>0.000052969910859573463</td><td colspan="2">-0.0002185649559977576</td><td>-0.00042291963429186286</td></tr>
<tr><td>6</td><td>0.000092946317790511788</td><td colspan="2">-0.0001528070357962874</td><td>-0.00010850751528468372</td></tr>
<tr><td>7</td><td>-0.00012033624991993779</td><td colspan="2">0.00011630243201915524</td><td>-0.00015977404954095609</td></tr>
<tr><td>8</td><td>0.00029546206646246159</td><td colspan="2">-0.00029660356997895931</td><td>0.00028222153383191534</td></tr>
<tr><td>9</td><td>-0.00064861599266253221</td><td colspan="2">0.00064873928601494324</td><td>-0.0006515159005454213</td></tr>
</table>

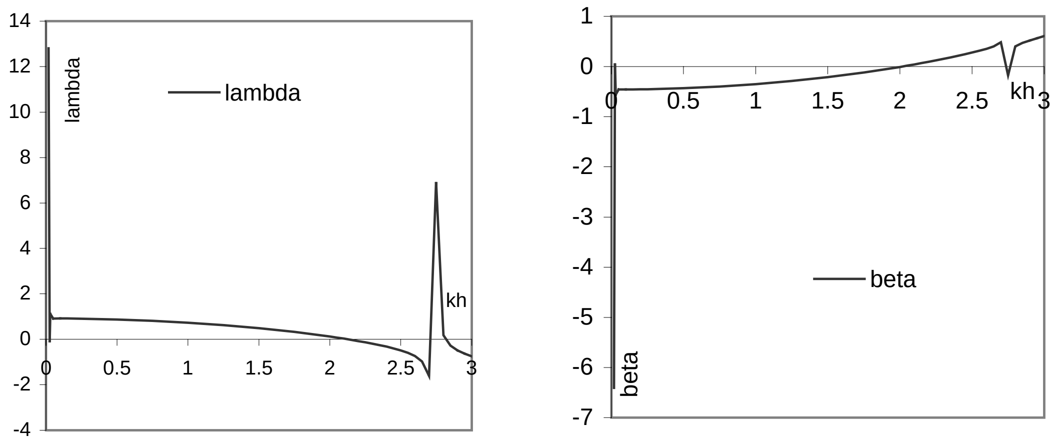

Figure 1 - λ and β parameters as a function of kh obtained with $\theta_1 = \frac{\pi}{16}$ and $\theta_2 = \frac{3\pi}{16}$.

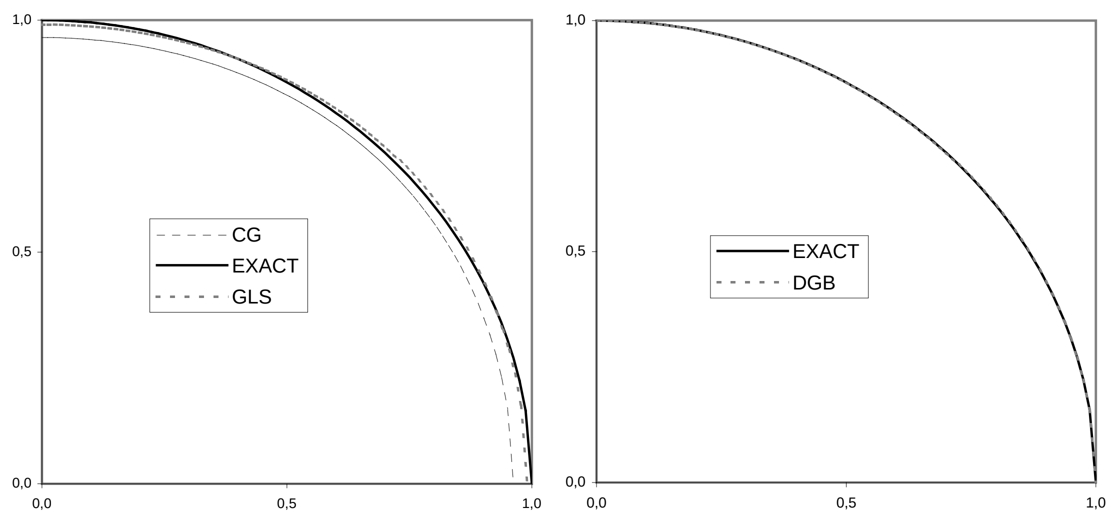

(a) *kh=1* (b) *kh=1*

Figure 2 - Dispersion relations for *kh=1*, (a) Continuous Galerkin (CG) and Galerkin Least Squares (GLS), (b) Discontinuous Bubble Galerkin formulation (DGB).

The first example treated here consists of solving the homogenous helmholtz Eq. (1) over a unity square domain submitted to Dirichlet boundary conditions. For that case, the exact solution is given by a plane wave propagating in θ-direction: $u(x, y) = \cos(k(x\cos\theta + y sin\theta))$. A study of the accuracy of approximate solutions is carried out for *k=100*, using an uniform finite element mesh (160 x 160) and varying the propagation direction by choosing the appropriate values for the boundary conditions. This analysis is presented in Fig. 3 where the relative errors of the present discontinuous finite element formulation (DGB) in L^2-norm and H^1-seminorm are compared to the corresponding errors of the continuous interpolant (CI), the Quasi-Stabilized Finite Element Method (QS) and the Galerkin Least Squares (GLS) solutions for *kh=0.625*. Since we have addopted the optimal values of the stabilization parameters, DGB and QS approximations are identical in this case and close to the continuous interpolant while the GLS solution presents large relative erros.

Figure 4 shows the nodal interpolant, Discontinuous Bubble and Galerkin Least Squares finite element solutions in sections *x=0.5* along the y direction obtained with the same mesh for *θ=(π/4)*, that is the *θ*-direction which corresponds to the largest "phase" error for Discontinuous Bubble solution. These results show clearly large pollution effect on the GLS solution and confirm the good performance of the DGB formulation with no significant difference when compared to the continuous interpolant.

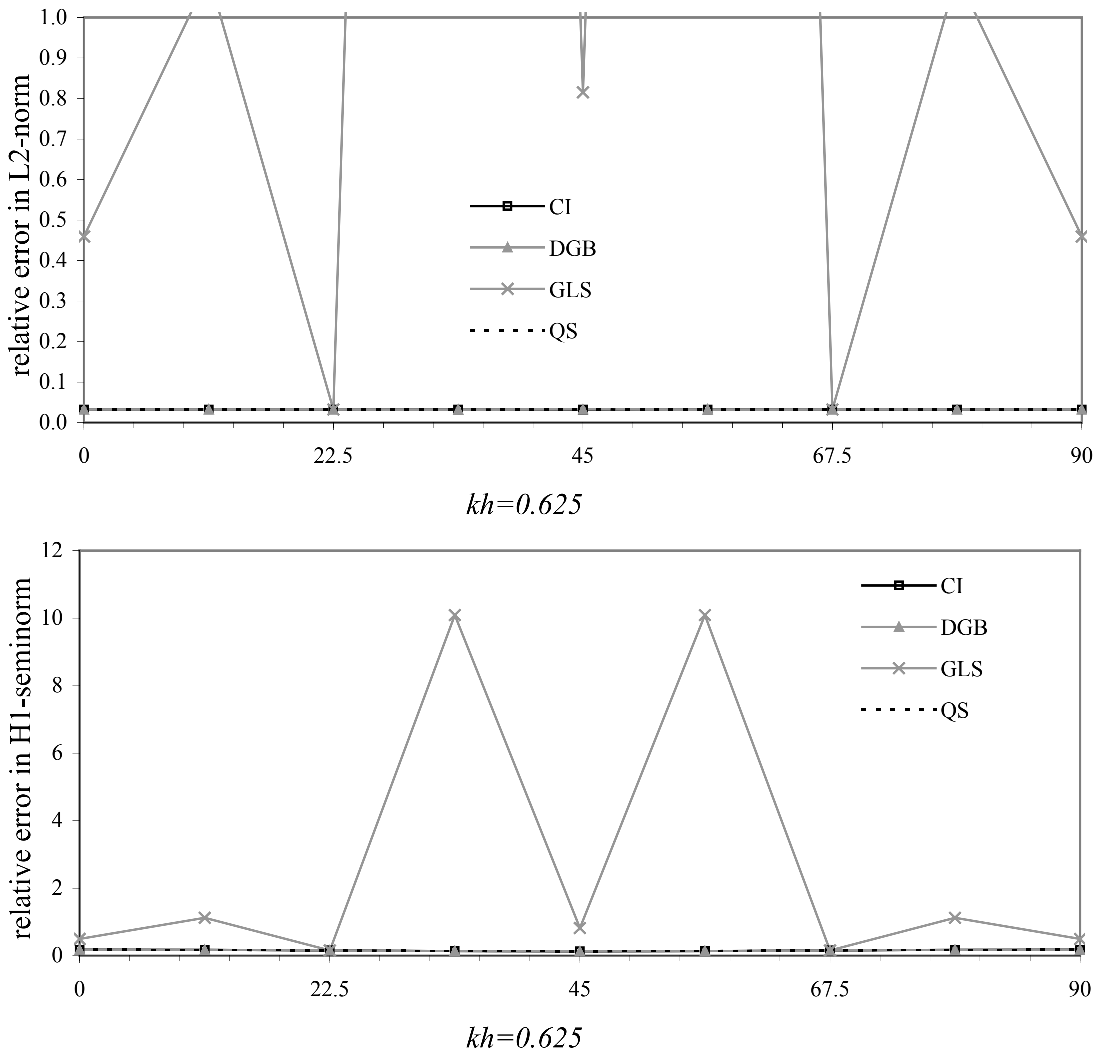

Figure 3 - Relative error of the discontinuous Galerkin solution (DGB) compared to the continuous interpolant (CI), Galerkin Least Squares (GLS) and Quasi Stabilized Finite Element Method (QS) in the L^2-norm and H^1-seminorm as a function of *θ*-direction for *k=100* with a *160x160* mesh.

The next example is similar to previous example, but now the exact solution is given by a superposition of *n* monoenergetic plane waves propagating in *n* different *θ*-directions: $u(x,y)=\sum_{i=1}^{n}\cos(k(x\cos\theta_i + y sin\theta_i))$. Firstly, three plane waves propagating in the directions $\theta_1 = 0,\ \theta_2 = \frac{\pi}{8},\ \theta_3 = \frac{\pi}{4}$. The relative errors in L^2-norm, H^1-seminorm and H^1-norm are present in Table 2. Figure 5 shows the nodal interpolant, Discontinuous Bubble and Galerkin Least Squares finite element solutions in sections *x=0.5* along the *y* direction . Figure 6 shows the same FEM solutions in section *y=0.5* along the *x* direction. Again, the results show the good performance of the DGB formulation and how this formulation reduces the phase error over all wave vector orientations θ.

Table 2. Realative errors of FEM: Example 2, three plane waves

	Relative Errors of finite element methods			
	CI	DGB	GLS	Galerkin
L^2-norm	3.22E-02	3.23E-02	5.40E-01	1.71E+00
H^1-seminorm	1.56E-01	1.56E-01	5.59E-01	1.72E+00
H^1-norm	1.56E-01	1.56E-01	5.59E-01	1.72E+00

Secondly, six plane waves propagating in the directions $\theta_1 = 0,\ \theta_2 = \frac{\pi}{20},\ \theta_3 = \frac{\pi}{10},\ \theta_4 = \frac{3\pi}{20},\ \theta_5 = \frac{\pi}{5},\ \theta_6 = \frac{\pi}{4}$. Figures 7 and 8 show the nodal interpolant, Discontinuous Bubble and Galerkin Least Squares finite element solutions in sections *x=0.5* and *y=0.5* respectively. Very similar conclusions to the previous example can be drawn. We should observe that, in these two examples the directions of plane waves propagations are always different to $\theta_1 = \frac{\pi}{16}$ and $\theta_2 = \frac{3\pi}{16}$, which are the optimal choice in Eq. (35-36) for the stabilization parameters.

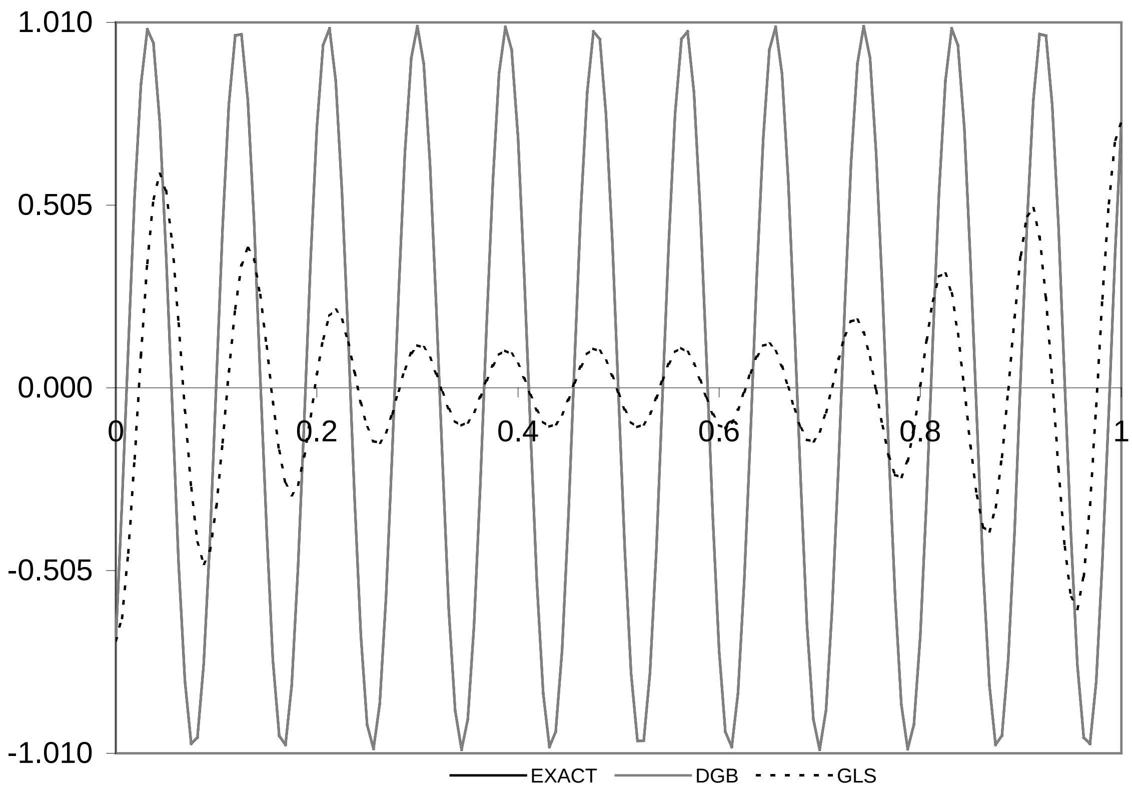

Figure 4 - DGB and GLS solutions of homogeneous problem in two dimension at sections *x=0.5*, *k=100*, *θ=(π/4)*.

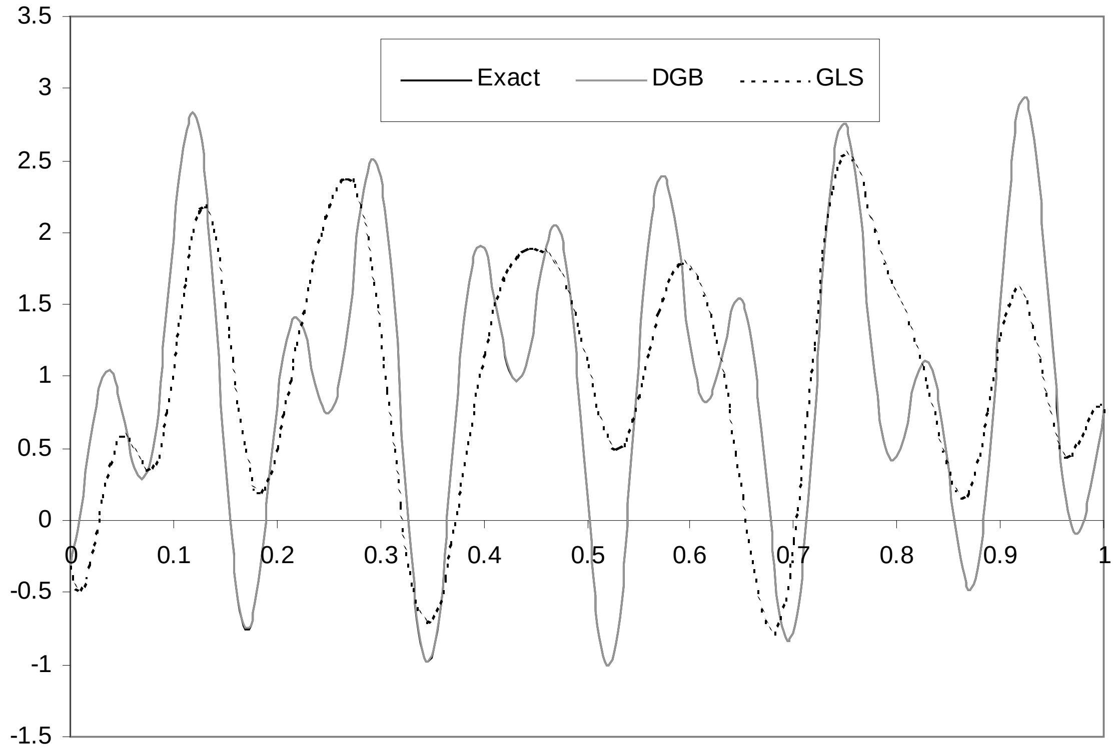

Figure 5 - DGB and GLS solutions of homogeneous problem in two dimension at sections *x=0.5*, *k=100*, three plane waves.

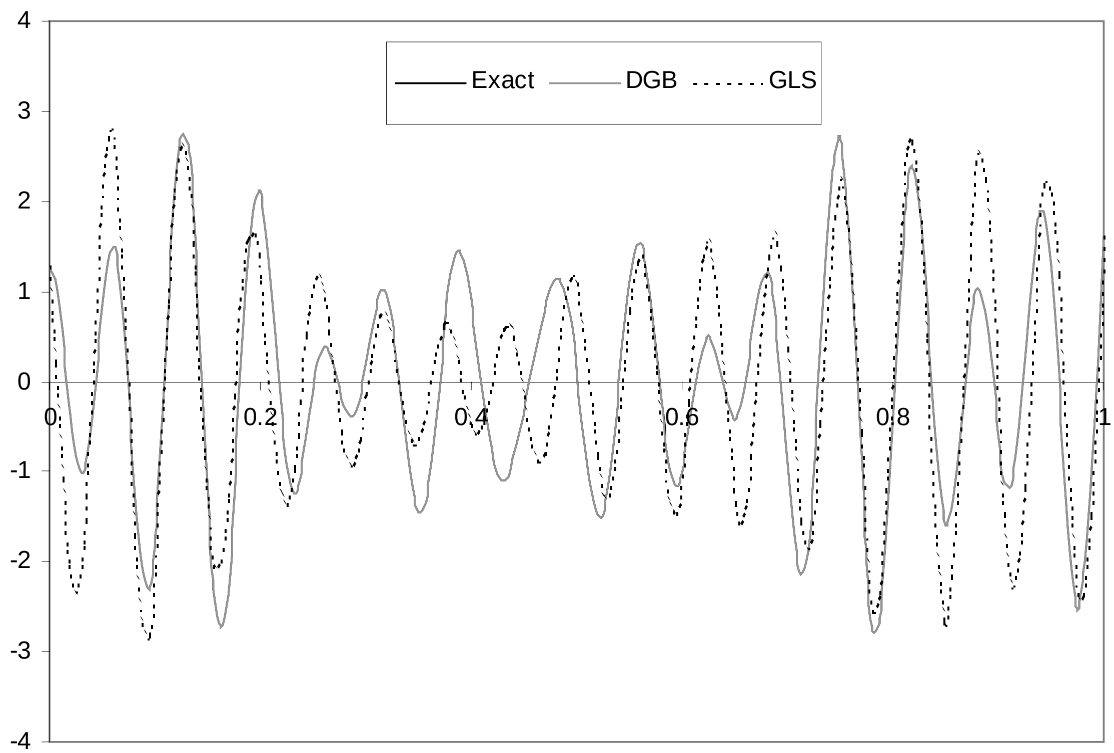

Figure 6 - DGB and GLS solutions of homogeneous problem in two dimension at sections *y=0.5*, *k=100*, three plane waves.

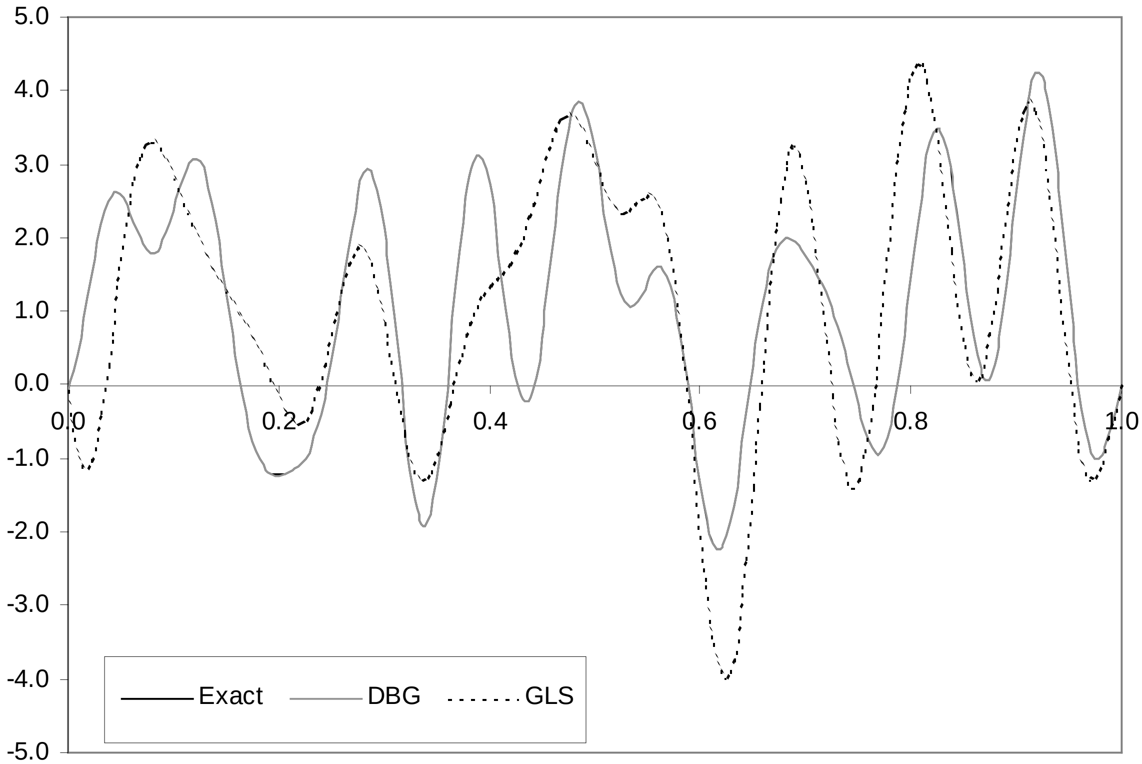

Figure 7 - DGB and GLS solutions of homogeneous problem in two dimension at sections *x=0.5*, *k=100*, six plane waves.

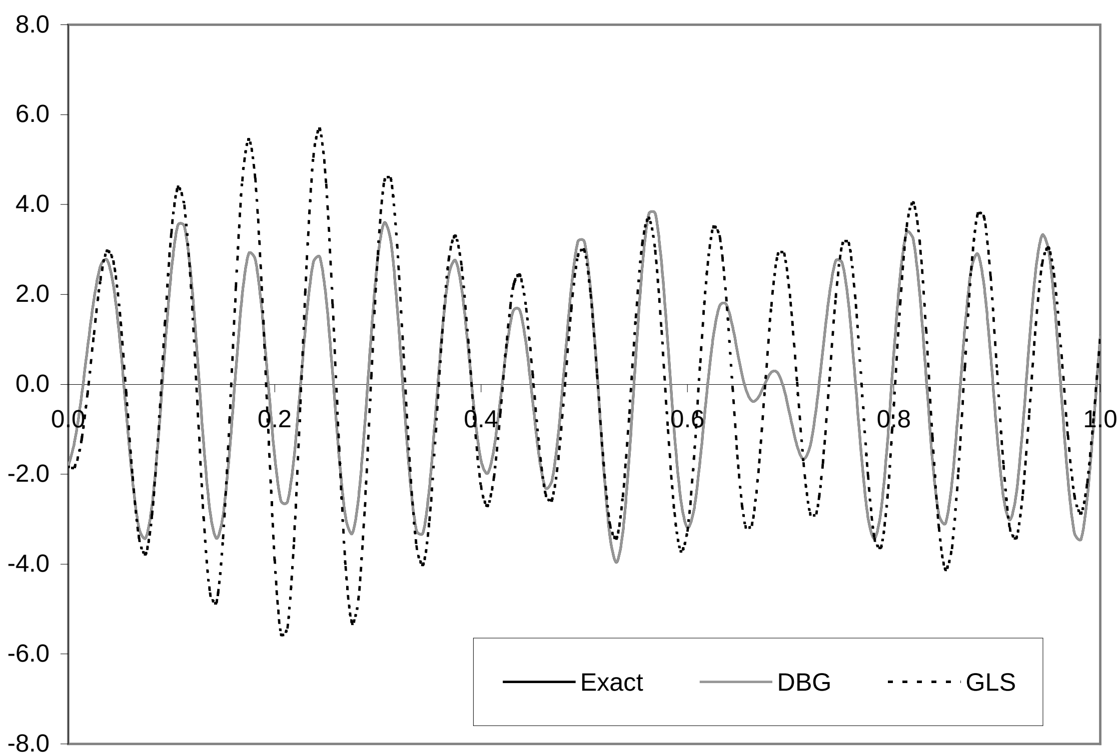

Figure 8 - DGB and GLS solutions of homogeneous problem in two dimension at sections *y=0.5*, *k=100*, six plane waves.

4. CONCLUSIONS

We present a new consistent discontinuous finite element formulation for the Helmholtz problem. Consistency derives from the fact that the exact continuous solution satisfies the discrete equation. The continuity is only relaxed on nodes placed on the interior of the elements instead across the element edges as it was admitted initially. The interior degrees of freedom are associated to discontinuous bubble functions, which are not necessarily higher-order polynomials, once those functions are to be zero on the element edges. From the computational standpoint, this represents a significant reduction of costs as the interior degrees of freedom might be eliminate using standard condensation techniques.

Moreover, discontinuous formulation proposed by the authors make use of two design parameters, which are selected to enhance accuracy and stability. In the present method, departing from the stencil obtained with the internal degrees condensation, we build a strategy for choosing those parameters aiming at matching the exact wave number in two different directions. This is conducted analytically for uniform meshes. The stencil of the Quasi Stabilized Finite Element Method is retrieved for the optimal choice of the stabilization parameters. Nevertheless, it is important to remark that in our case, the final problem is derived from a consistent variational formulation, which allows the enforcement of generic boundary conditions and the use of non structured meshes as well. In this last case, the analytical way of obtaining the parameters would be no longer available.

A number of numerical simulations involving acoustic problems is presented in order to assess the good performance of the proposed formulation. We understand that those results not only confirm the improvement on the approximations involving the Helmholtz equation but also estimulates the development of formulations containing the discontinuous bubbles for different applications.

Acknowledgements

The authors wish to thank the Brazilian research-funding agencies CNPq and FAPESB for their support to this work.

REFERENCES

Alvarez, G. B., Loula, A. F. D., Dutra do Carmo, E. G. and Rochinha, F. A., submitted. A discontinuous finite element formulation for the Helmholtz equation. *Comput. Methods Appl. Mech. Engrg.*

Babuška, I., Ihlenburg, F., Paik, E.T. and Sauter, S.A., 1995. A generalized finite element method for solving the Helmholtz equation in two dimensions with minimal pollution. *Comput. Methods Appl. Mech. Engrg.*, vol. 128, pp. 325-359.

Dutra do Carmo, E. G. and Duarte, A. V. C., 2002. New formulations and numerical analysis of discontinuous Galerkin methods. *Computational and Applied Mathematics*, vol. 21, No. 3, pp. 661-715.

Farhat, C., Macedo, A.P. and Lesoinne, M., 2000. A two-level domain decomposition method for the iterative solution of high frequency exterior Helmholtz problems. *Numer. Math.*, vol. 85, pp. 283-308.

Farhat, C., Harari, I. And Franca, L., 2001. The discontinuous enrichment method. *Comput. Methods Appl. Mech. Engrg.*, vol. 190, pp. 6455-6479.

Farhat, C., Harari, I. and Hetmaniuk, U., 2003. A discontinuous Galerkin method with Lagrange multipliers for the solution of Helmholtz problems in the mid-frequency regime. *Comput. Methods Appl. Mech. Engrg.*, vol. 192, pp. 1389-1419.

Franca, L.P., Farhat, C., Macedo, A.P. and Lesoinne, M., 1997. Residual-free bubbles for the Helmholtz equation. *Int. J. Numer. Methods Engrg.*, vol. 40, pp. 4003-4009.

Franca, L. P. and Macedo, A. P., 1998. A two-level finite element method and its application to the Helmholtz equation. *Int. J. Numer. Methods Engrg.*, vol. 43, No. 1, pp. 23-32.

Harari, I. and Hughes, T.J.R., 1991. Finite element method for the Helmholtz equation in an exterior domain: Model problems. *Comp. Meth. Appl. Mech. Eng.*, vol. 87, pp. 59-96.

Harari, I. and Hughes, T.J.R., 1992. Galerkin/least squares finite element methods for the reduced wave equation with non-reflecting boundary conditions in unbounded domains. *Comp. Meth. Appl. Mech. Eng.*, vol. 98, pp. 411-454.

Hughes, T. J. R., 1995. Multiscale phenomena: Green's functions, the Dirichlet-to-Neumann formulation, subgrid scale models, bubbles and the origins of stabilized methods. *Comput. Methods Appl. Mech. Engrg.*, vol. 127, No. 1/4, pp. 387-401.

Ihlenburg, F. and Babuška, I., 1995. Finite element solution of the Helmholtz equation with high wave number Part I: The h-version of the FEM. *Comput. Math. Appli.*, vol. 30, No. 9, pp. 9-37.

Loula, A. F. D., Alvarez, G. B., Dutra do Carmo, E. G. and Rochinha, F. A., submitted. A discontinuous finite element method at element level for Helmholtz equation. *Comput. Methods Appl. Mech. Engrg.*

Thompson, L.L. and Pinsky, P.M., 1995. A Galerkin least squares finite element method for the two-dimensional Helmholtz equation. *Int. J. Numer. Methods Eng.*, vol. 38, No. 3, pp. 371-397.